Journal of Computational Physics 232 (2013) 87–99

Contents lists available at SciVerse ScienceDirect

Journal of Computational Physics

journal homepage: www.elsevier.com/locate/jcp

A solution of the Boltzmann equation in the presence of inelastic collisions

I.N. Shishkova [a], S.S. Sazhin [b,*], J.-F. Xie [b]

[a] Low Temperature Department, Moscow Power Engineering Institute, Krasnokazarmennaya 14, Moscow 111250, Russia
[b] Sir Harry Ricardo Laboratories, Centre for Automotive Engineering, School of Computing, Engineering and Mathematics, Faculty of Science and Engineering, University of Brighton, Brighton BN2 4GJ, UK

ARTICLE INFO

Article history:
Received 9 June 2011
Received in revised form 2 March 2012
Accepted 3 July 2012
Available online 20 July 2012

Keywords:
Boltzmann equations
Collisions
Shock waves
Heat transfer
Evaporation
Kinetic modelling

ABSTRACT

The effect of inelastic collisions between two molecules on the solution of the Boltzmann equation is taken into account by presenting the change of state of molecules after collisions as a random (with uniform probability distribution) movement along a surface of an N-dimensional sphere, the squared radius of which is equal to the total energy of the molecules before and after the collision in the reference system of the centre of mass. The projection of a point on the surface of this sphere in each of N directions gives the root square of the kinetic energy in one of three directions in the physical space, or the internal energy of one of degrees of freedom, of one of two molecules. The kinetic energies of two molecules are described by the first six dimensions of the system, and the remaining $(N-6)$ dimensions describe the internal energies. This approach is applied to three test problems: shock wave structure in nitrogen, one-dimensional heat transfer through a mixture of n-dodecane and nitrogen and one-dimensional evaporation of n-dodecane into nitrogen. In the first problem, the predictions of the model are shown to be close to experimental data and also to the predictions of the earlier developed model, based on a different approach to taking into account the effects of inelastic collisions. The predicted heat flux for the second problem and mass flux for the third problem are shown to be very weak functions of the number of internal degrees of freedom when this number exceeds about 15. These results open the way for considering systems with arbitrarily large numbers of internal degrees of freedom by reducing the analysis of these systems to the analysis of systems with relatively small numbers of internal degrees of freedom.

1. Introduction

A widely used engineering approach to modelling evaporation/condensation processes is based on the hydrodynamic approximation (see [22]). The limitation of this approach, even in the case of evaporation at high pressures, has been discussed in a number of papers, including [16,29,27,23,28]. In these papers the evaporation of n-dodecane $C_{12}H_{26}$ (the nearest approximation for Diesel fuel) has been considered and a new model for the analysis of droplet heating and evaporation has been developed based on a combination of the kinetic and hydrodynamic approaches. In the immediate vicinity of droplet surfaces (up to about 100 molecular mean free paths), the vapour and ambient gas dynamics have been studied based on the Boltzmann equation (kinetic region), while at larger distances the analysis has been based on the hydrodynamic equations (hydrodynamic region). Mass, momentum and energy fluxes have been conserved at the interface between these regions.

The model developed in these papers is based on a number of assumptions, the most serious of which is that the contribution of inelastic collisions has been ignored. This assumption could have been justified in the case of mono-atomic

* Corresponding author.
E-mail address: S.Sazhin@brighton.ac.uk (S.S. Sazhin).

0021-9991/$ - see front matter © 2012 Elsevier Inc. All rights reserved.
http://dx.doi.org/10.1016/j.jcp.2012.07.007

molecules, but appears to be highly questionable in the case of such complex molecules as $C_{12}H_{26}$ considered in the above mentioned papers. Even if the analysis of the dynamics of these molecules is simplified by considering the United Atom Model (see [7,34] for details), the number of internal degrees of freedom of this molecule is expected to exceed 100. There seems to be no justification for ignoring their contribution.

Perhaps the first phenomenological model for binary collisions in a gas mixture having continuous internal energy was developed by [6]. This model was applied to Monte Carlo simulation of rarefied gas flows. Since the publication of this pioneering paper, a substantial number of papers have been published, in which various models of inelastic collision have been considered. Without making any attempt to present an extensive list of these papers we mention [33,14,9,4,5,3,8,10,21,30,17,15,11]. This list does not include papers where the models for collisions of specific atoms and molecules have been considered, such as H_2–H_2 collisions [35], N–N_2 collisions [12] and H–N_2 collisions [31]. Also, it does not include papers where the effects of inelastic collisions on transport coefficients are considered (e.g. [20]).

The model suggested in this paper is different from those suggested earlier, although it is based on some widely used assumptions, such as the approximation of molecules by inelastic hard spheres (IHS). Although this model has been tested for some rather specific problems, its nature is rather general and it can be applied to any molecules with arbitrary large numbers of internal degrees of freedom. This model is expected to be the most effective for the analysis of such complex molecules as n-dodecane, considered in our previous papers.

Basic ideas of the new model are discussed in Section 2. In Section 3 this model is applied to the analysis of three test cases. The main results of the paper are summarised in Section 4.

2. Mathematical model

2.1. A model for inelastic collisions

As in our previous papers [29,27,23,28], we assume that the molecules can be approximated as hard spheres. In contrast to these papers, however, we take into account the inelastic effects during the collisions of these spheres, using a well known inelastic hard spheres (IHS) model (see [21]). As in [29,27,23,28] only the effects of binary collisions are taken into account. This is justified by the fact that the Boltzmann equation is solved in a very thin layer, the thickness of which is typically about 10 mean free paths.

Let us consider two colliding molecules. Regardless of the nature of the collision between them, their centre of mass is not affected by this collision. The state of the molecules after the collision is described in the reference system linked with this centre of mass. In this system, each of these molecules has three translational and a certain number of internal degrees of freedom, so that the total number of degrees of freedom of both molecules is equal to N. During the collisions, the energies of each molecule are redistributed between the degrees of freedom, but the total number of degrees of freedom remains the same. Let us assume that none of these degrees of freedom has any preference over the others. This assumption implies that we focus our attention on the systems close to thermodynamic equilibrium. The model is not applicable to the systems in the states far from thermodynamic equilibrium, such as gas lasers (see [25,26]). Possible generalisation of the model to the case when this assumption is not valid is discussed in the last paragraph of this section.

This assumption allows us to consider the redistribution of energy between these degrees of freedom during the collision process as random with uniform probability distribution. For each of these degrees of freedom we allocate one dimension in the N-dimensional space describing all degrees of freedom. Once we have done this, we consider a sphere in this space with its centre at the origin (where energies of all degrees of freedom are equal to 0) and radius given by the following expression:

$$r = \sqrt{\sum_{i=1}^{i=N} E_i}, \tag{1}$$

where E_i is the energy of the ith degree of freedom (translational or internal). Since r^2 gives the total energy of the system E_f, Eq. (1) can be considered as an equation of the conservation of energy at the surface of the sphere in the centre of mass system of reference.

Introducing the new coordinates $x_i = \pm\sqrt{E_i}$, we can consider an N-dimensional vector

$$\mathbf{X} = (x_1, x_2, \ldots, x_N)$$

with the basis $(\mathbf{e_1}, \mathbf{e_2}, \ldots, \mathbf{e_N})$ and the norm $||\mathbf{X}|| = r = \sqrt{E_f}$, where E_f is the total energy of the system. The norms of all vectors $\mathbf{e_i}$ are equal to one and these vectors are mutually perpendicular.

The redistribution of energy between the degrees of freedom during the collision process can be described in terms of the rotation of vector $\mathbf{X}$ in the N-dimensional space. For $N = 3$ this is schematically shown in Fig. 1. If none of the degrees of freedom has any preference over the others, then this rotation of the vector $\mathbf{X}$ can be considered as random with uniform probability distribution. In the most general form it can be described by the following equation:

$$\mathbf{X}' = \mathbf{A}\mathbf{X}, \tag{2}$$

where $\mathbf{X}'$ is the new position of vector $\mathbf{X}$ after rotation, $\mathbf{A}$ is the rotation matrix:

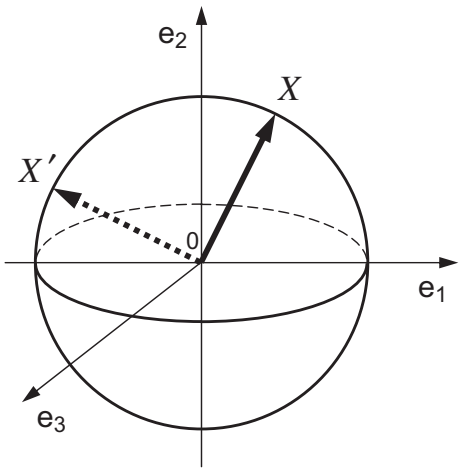

Fig. 1. A schematic presentation of the rotation of vector **X** in the three dimensional space ($\mathbf{e}_1, \mathbf{e}_2, \mathbf{e}_3$).

$$\mathbf{A} = \begin{bmatrix} a_{11} & a_{12} & \cdots & a_{1N} \\ a_{21} & a_{22} & \cdots & a_{2N} \\ \cdots & \cdots & \cdots & \cdots \\ a_{N1} & a_{N2} & \cdots & a_{NN} \end{bmatrix}.$$

The conservation of the total energy during the collision process implies that vector $\mathbf{X}'$ remains at the surface of the sphere of radius r. This is possible if and only if

$$\mathbf{A}^{\mathrm{T}}\mathbf{A} = \mathbf{E}, \tag{3}$$

where $\mathbf{A}^{\mathrm{T}}$ is the transpose of the matrix **A**, **E** is the unit matrix

$$\mathbf{E} = \begin{bmatrix} 1 & 0 & \cdots & 0 \\ 0 & 1 & \cdots & 0 \\ \cdots & \cdots & \cdots & \cdots \\ 0 & 0 & \cdots & 1 \end{bmatrix}.$$

Eq. (3) can be presented in a more explicit form as the combination of the following systems of equations

$$\left.\begin{array}{llll} a_{11}^2+ & a_{21}^2+ & \cdots & +a_{N1}^2 = 1 \\ a_{12}^2+ & a_{22}^2+ & \cdots & +a_{N2}^2 = 1 \\ \cdots & \cdots & \cdots & \cdots \\ a_{1N}^2+ & a_{2N}^2+ & \cdots & +a_{NN}^2 = 1 \end{array}\right\}, \tag{4}$$

$$\left.\begin{array}{llll} a_{11}a_{12}+ & a_{21}a_{22}+ & \cdots & +a_{N1}a_{N2} = 0 \\ a_{11}a_{13}+ & a_{21}a_{23}+ & \cdots & +a_{N1}a_{N3} = 0 \\ \cdots & \cdots & \cdots & \cdots \\ a_{11}a_{1N}+ & a_{21}a_{2N}+ & \cdots & +a_{N1}a_{NN} = 0 \end{array}\right\}, \tag{5}$$

$$\left.\begin{array}{llll} a_{12}a_{13}+ & a_{22}a_{23}+ & \cdots & +a_{N2}a_{N3} = 0 \\ a_{12}a_{14}+ & a_{22}a_{24}+ & \cdots & +a_{N2}a_{N4} = 0 \\ \cdots & \cdots & \cdots & \cdots \\ a_{12}a_{1N}+ & a_{22}a_{2N}+ & \cdots & +a_{N2}a_{NN} = 0 \end{array}\right\}, \tag{6}$$

. . . . . .

$$a_{1(N-1)}a_{1N} + a_{2(N-1)}a_{2N} + \cdots + a_{N(N-1)}a_{NN} = 0. \tag{7}$$

When writing Eqs. (5)–(7) identical equations have been excluded. The total number of Eqs. (5)–(7) is

$$(N-1) + (N-2) + (N-3) + \cdots + 1 = \frac{N}{2}(N-1)$$

for N^2 unknown coefficients a_{ij}. This allows us to take randomly $N^2 - \frac{N}{2}(N-1) = \frac{N}{2}(N+1)$ of these coefficients with an additional restriction imposed by Eq. (4) (normalisation condition).

The following algorithm for the construction of the matrix **A** is suggested.

1. The coefficients $a_{11}, a_{21}, \ldots, a_{N1}$ are arbitrarily chosen but normalised based on the first equation in System (4).
2. The coefficients $a_{12}, a_{22}, \ldots, a_{(N-1)2}$ are arbitrarily chosen, while the value of the coefficient a_{N2} is found from the first equation of System (5):

$$a_{N2} = -\frac{1}{a_{N1}}\left(a_{11}a_{12} + a_{21}a_{22} + \cdots + a_{(N-1)1}a_{(N-1)2}\right). \tag{8}$$

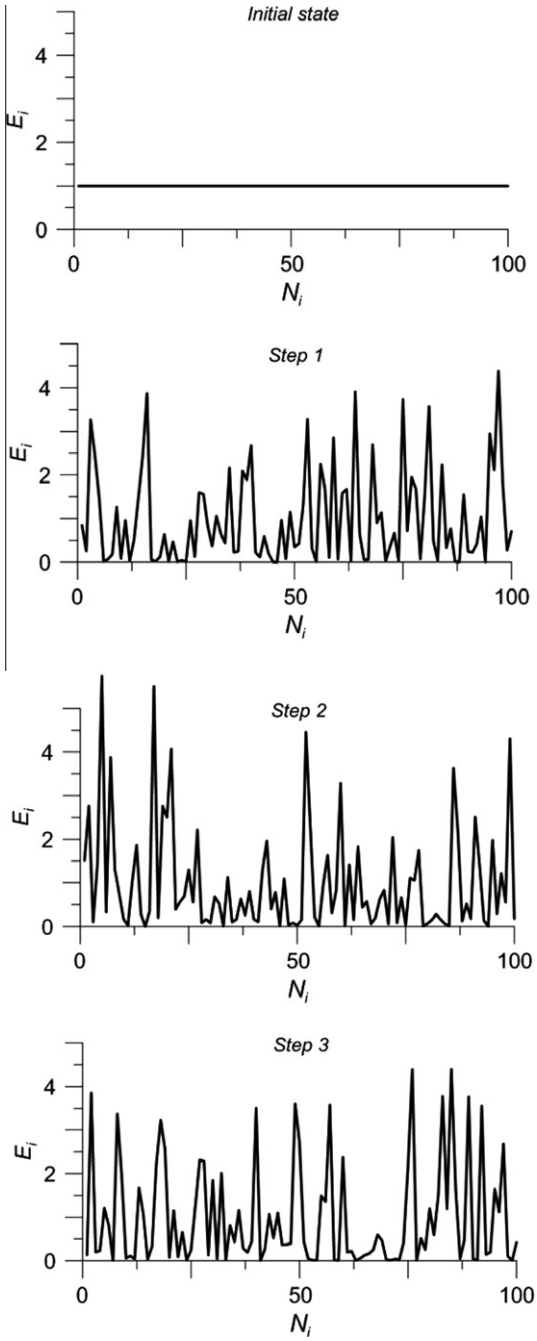

Fig. 2. The values of energies of individual degrees of freedom (E_i) versus N_i at the initial state and after Steps 1–3.

Then all coefficients are normalised based on the second equation in System (4).

3. The coefficients $a_{13}, a_{23}, \ldots, a_{(N-2)3}$ are arbitrarily chosen, while the value of the coefficients $a_{(N-1)3}$ and a_{N3} are found from the solution of the second equation in System (5) and the first equation in System (6). These equations can be rearranged as:

$$\left.\begin{array}{ll} a_{(N-1)1}a_{(N-1)3}+ & a_{N1}a_{N3} = b_{13} \\ a_{(N-1)2}a_{(N-1)3}+ & a_{N2}a_{N3} = b_{23} \end{array}\right\}, \tag{9}$$

where

$$b_{13} = -\left(a_{11}a_{13} + a_{21}a_{23} + \cdots + a_{(N-2)1}a_{(N-2)3}\right),$$

$$b_{23} = -\left(a_{12}a_{13} + a_{22}a_{23} + \cdots + a_{(N-2)2}a_{(N-2)3}\right).$$

Then all coefficients are normalised based on the third equation in System (4).

Following the same procedure all other components of the matrix $\mathbf{A}$ are found, and this allows us to calculate $\mathbf{X}'$ based on Eq. (2). An example of the temporal evolution of the system with 100 degrees of freedom is shown in Fig. 2. The ordinate axis in this figure shows the energies E_i referring to individual degrees of freedom N_i ($i \in [1, 100]$). Initially all degrees of freedom have energies equal to 1 ($E_i = 1$). This is shown in the top part of this figure (Initial state). After the first step energies E_i acquire random values in the range from 0 to 5, but the sum of all E_i remains the same as at the initial state ($\sum_{i=1}^{i=100} E_i = 100$). The nature of the distribution of E_i remains random after steps 2 and 3 although with different values of individual energies. In principle, the value of one E_i can reach the maximal value of 100, provided that all other E_i are equal to 0, although this has been never observed in our simulations.

The model described above could be generalised to the case when the probabilities of excitation of various degrees of freedom are not equal. This could be achieved by introduction of the weighting function, and/or limiting the range of degrees of freedom to be activated. We cannot, however, specify this weighting function in the case of such complex molecules as n-dodecane, for which our model has been primarily developed, or even justify the need to introduce this function in this case.

2.2. An algorithm for the solution of the Boltzmann equation

Following [2], the numerical solution of the Boltzmann equation (for one or several components) is performed in two steps. Firstly, molecular displacements are calculated ignoring the effect of collisions. Secondly, the collisional relaxation is calculated under the assumption of spatial homogeneity.

Ignoring the effects of collisions, the discretised form of the Boltzmann equation, describing molecular displacements, for each component can be presented as

$$\frac{\Delta f}{\Delta t} + \mathbf{v}\frac{\Delta f}{\Delta \mathbf{r}} = 0, \tag{10}$$

where $f \equiv f(\mathbf{v}, \mathbf{r}, t)$ is the distribution function for the velocity ($\mathbf{v}$) and physical spaces ($\mathbf{r}$).

In this case, the total internal energy in each velocity range should be conserved, which implies that

$$\frac{\Delta(E_{\text{int}} f)}{\Delta t} + \mathbf{v}\frac{\Delta(E_{\text{int}} f)}{\Delta \mathbf{r}} = 0, \tag{11}$$

where $E_{\text{int}} \equiv E_{\text{int}}(\mathbf{v}, \mathbf{r}, t)$ are internal energies of molecules with given $\mathbf{v}$ and $\mathbf{r}$ at time t.

A model for inelastic collisions, described in the previous section, allows us to obtain the energies of all degrees of freedom after individual collisions as illustrated in Fig. 2. However, we are interested only in the net change of the kinetic energy of each of two molecules during collisions in the centre of mass reference system. This change of the kinetic energy can be described in terms of the change of the radius of the three dimensional sphere, which is the projection of the N-dimensional sphere, described in the previous section, on the three-dimensional space, describing the kinetic energies of both colliding molecules in three directions. This is schematically illustrated in Fig. 3 for the case of the projection of the N-dimensional sphere on the two-dimensional plane. Following [29], this space is presented in terms of the components of momenta p_x and p_y of both colliding molecules. Points p and p_* show the positions of molecules before the collision. If the collisions were elastic, then the values of momenta after collisions would lie on the dashed circle shown in Fig. 3, being separated by 180°. Possible values of these momenta after the collisions are shown as empty circles.

As mentioned in [29], randomly chosen directions of molecular momenta after collision are likely to lead to the values of these momenta lying between the values in the nodes of the discretised momenta space. This eventually can lead to non-conservation of momenta and energies during the collision process. To overcome this problem, following [29] the momenta are discretised not only during the description of molecular motion but also in the analysis of the collision process. Namely, we assume that the momenta after the collisions belong to an *a priori* chosen set of momenta, which are nodes in the momenta space shown in Fig. 3. This is achieved by moving the actual point on the surface of the sphere to the nearest node. Since the nodes are not uniformly distributed on the surface of the sphere in the general case, this leads to partial loss of

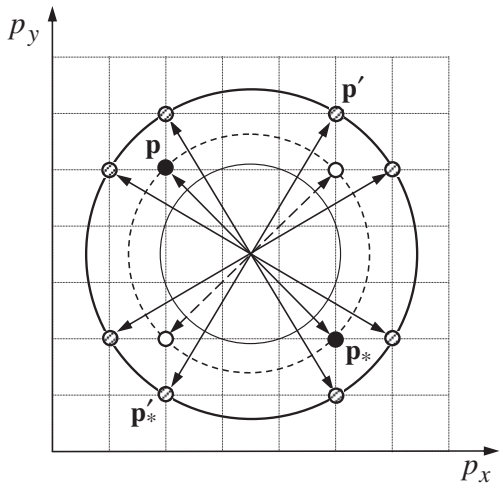

Fig. 3. A projection of the surface of an N-dimensional sphere, describing the energies referring to translational and internal degrees of freedom of two colliding molecules, into a two dimensional space referring to two translational degrees of freedom. p and p_* show the locations of the molecular momenta before the collision. The dashed circle shows possible locations of molecular momenta after the collision if the contribution of internal degrees of freedom is ignored. The thin solid circle shows possible locations of molecular momenta after the collision if molecular internal energy increases during the collision. The thick solid circle shows possible locations of molecular momenta after the collision if molecular internal energy decreases during the collision. p' and p'_* show the allowed locations of the molecular momenta after the collision if molecular internal energy decreases during the collision.

randomness of the distribution of momenta after collisions. This is one of the weaknesses of the model under consideration, but seems not to lead to serious limitations of the range of its applicability as demonstrated in Section 3.

In the case shown in Fig. 3, in the absence of inelastic collisions, there are four such *nodes* corresponding to four combinations of momenta of molecules after collision. The maximal number of these combinations for the plane is 8. In the three dimensional case, the circumferences shown in Fig. 3 turn into the surfaces of spheres and the maximal number of possible intersection points increases to 24. This corresponds to the maximal total number of combinations of momenta after collision. This approach provides the consistency in discretisation processes used for the description of molecular dynamics and collision processes. It has been tested on numerous problems, some of which are discussed in [29].

If during the collision the net internal energy of molecules increases, this has to be compensated for by the decrease in the kinetic energies of molecules, and the radius of the corresponding circle in Fig. 3 is decreased. In the opposite case, when the net internal energy of molecules decreases, this has to be compensated for by the increase in the kinetic energies of molecules, and the radius of the corresponding circle in Fig. 3 is increased. Both cases are shown in Fig. 3. In the case of increased net kinetic energy of molecules, possible values of the momenta of both molecules after the collision are shown as the grey circles. These include points p' and p'_*. The changes of radii of the circles after collision have been calculated based on Korobov's sequences [13,18], enhanced by the randomisation of individual points. As in the case of elastic collisions, the points p' and p'_* are chosen to coincide with the nodes of the discretised momenta space.

3. Applications

The model described in the previous section has been tested using three simple one-dimensional examples. These are shock wave structure in nitrogen, heat flux between two parallel plates in a mixture of n-dodecane and nitrogen and one-dimensional evaporation of n-dodecane into nitrogen.

3.1. Shock wave structure

The first test is focused on the prediction of the shock wave structure observed experimentally [1]. In this paper the results of accurate measurements of the density distribution in argon and nitrogen shock waves are presented. These measurements were performed in a shock tube for Mach numbers ranging from 1.55 to 9 (argon) and from 1.55 to 10 (nitrogen) by the absorption of an electron beam. Our focus will be on the results referring to nitrogen with Mach number equal to 2 for the parameters before the shock wave. Using the Rankine–Hugoniot relationships, this leads to the following ratios of number densities $n_\pm$, static temperatures $T_\pm$ and velocities $v_\pm$ after and before the shock wave at large distances from it (indicated by subscripts $+$ and $-$ respectively) [19]:

$$\frac{n_+}{n_-} = 2.2857; \quad \frac{T_+}{T_-} = 2.0781; \quad \frac{v_+}{v_-} = 0.4375.$$

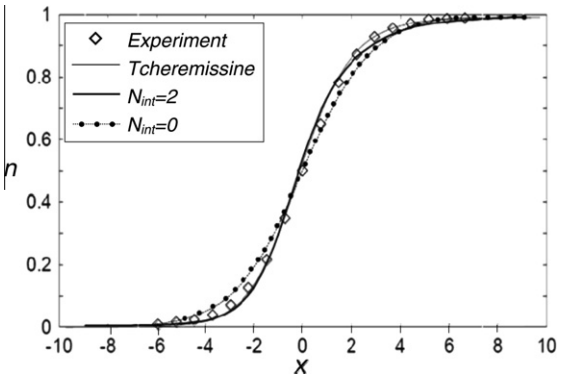

Fig. 4. Plots of $n = (n_n - n_-)/(n_+ - n_-)$, where n_n is the current number density of nitrogen, versus the distance x normalised by the mean free path $\ell = (\sqrt{2}\pi\sigma_{N_2}^2 n_-)^{-1}$, where σ_{N_2} is the characteristic diameter of N_2 molecules. $x = 0$ shows the location of the shock wave. The dotted curve refers to the results of our calculations when the contribution of the internal degrees of freedom is ignored; the thick solid curve refers to the results of our calculations when the contribution of the internal degrees of freedom is taken into account; the thin solid curve refers to the results of calculations reported by [32], taking into account the contribution of the internal degrees of freedom; rhombuses show the experimental results reproduced from [1].

Rotational relaxation in nitrogen is found to be very fast for all Mach numbers [1]. Consequently the coupling between rotational and translational relaxation is expected to be very strong. Since the vibrational degrees of freedom could be ignored for the conditions of the experiment, we consider only two internal degrees of freedom referring to the rotational motion ($N_{\text{int}} = 2$).

The calculations have been performed for the normalised density $n = (n_n - n_-)/(n_+ - n_-)$, where n_n is the current number density of nitrogen, taking into account and ignoring these two internal degrees of freedom. The results are shown in Fig. 4. In the same figure, the experimental data, obtained in [1] (see his Fig. 11), and the modelling results reported in [32], are shown. Note that the approach used in [32] is different from the one described earlier in this paper, although it also takes into account the contribution of inelastic collisions. As follows from this figure, although the curves referring to the cases with and without taking into account the internal degrees of freedom show similar trends, the actual values of number densities predicted by both approaches are visibly different. Thus, ignoring the contribution of the internal degrees of freedom, an approach widely used by the researchers in this area, including those from our group (e.g. [29,27,23,28]), can be too crude a method for many engineering applications. Also, the results of our calculations, taking into account the contribution of the internal degrees of freedom, appear to be very close to experimental data and the modelling results reported in [32]. This gives us confidence in our approach to modelling this phenomenon.

In Fig. 5 we have presented the results of calculations of a hypothetical case, when nitrogen is allowed to have less or more than two internal degrees of freedom (N_{int}). The cases of $N_{\text{int}} = 0, 2, 6$ and 10 have been considered. As follows from this figure, the increase in the number of internal degrees of freedom from 0 to 2 and from 2 to 6 visibly affects the solution. However, further increase in this number from 6 to 10 produces only a relatively minor effect. This potentially opens the way for modelling systems with large numbers of internal degrees of freedom, by taking into account the contribution of a relatively small number of these degrees of freedom. This idea is supported by the tests considered in the next two subsections.

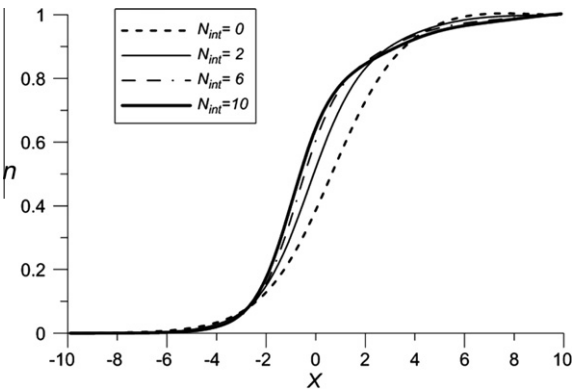

Fig. 5. Plots of $n = (n_n - n_-)/(n_+ - n_-)$ versus the distance x normalised by the mean free path ℓ of N_2 molecules showing the results of our calculations when the contribution of the various numbers of internal degrees of freedom N_{int} are taken into account.

3.2. Heat flux between two parallel plates

Let us consider two parallel plates at normalised temperatures $T_{w1} = 1.5$ and $T_{w2} = 1$; the space between these plates is filled with a mixture of n-dodecane $C_{12}H_{26}$ and nitrogen N_2 at the initial normalised temperature $T = 1$. The normalised number densities of both components are assumed initially equal to 1 ($n_d \equiv n_{C_{12}H_{26}} = n_n \equiv n_{N_2} = 1$). The distance between the plates is $L = 5\ell$, where ℓ is the average free molecular path at $n_{C_{12}H_{26}} = n_{N_2} = 1$ and $T = 1$. The problem setup is schematically presented in Fig. 6. Both components are calculated, using two Boltzmann equations as described in [29]. The

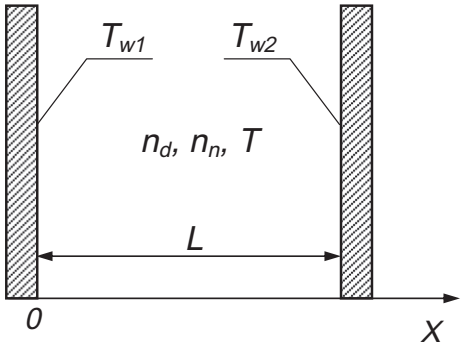

Fig. 6. A schematic presentation of the setup used for the analysis of the heat flux between two parallel plates, separated by the distance L along the x-axis and kept at temperatures T_{w1} and T_{w2}. n_d and n_n are number densities of n-dodecane and nitrogen respectively; $T \equiv T(x)$ is the temperature between the plates.

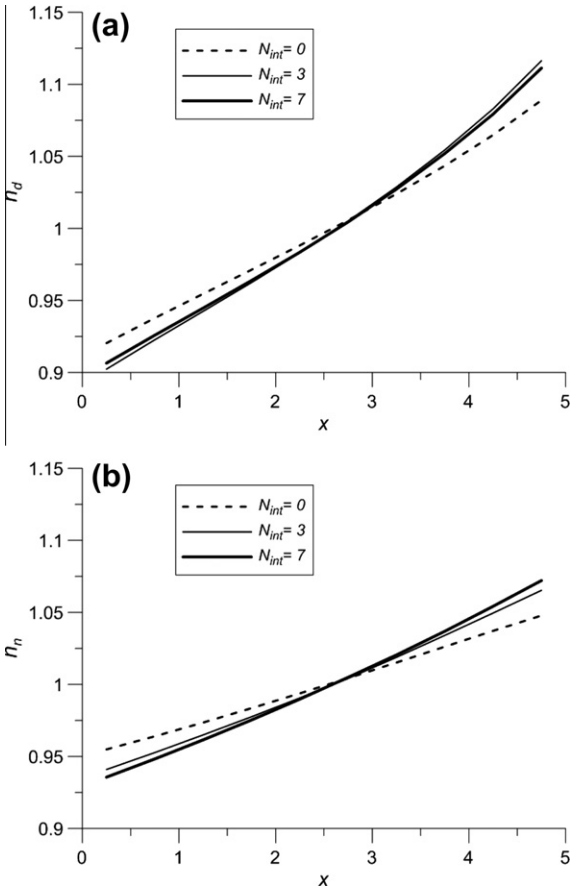

Fig. 7. Plots of n_d (a) and n_n (b) versus the distance x normalised by the mean free path ℓ for three values of N_{int} for the setup shown in Fig. 6. $x = 0$ shows the location of the left-hand side plate.

calculations have been performed assuming that nitrogen has no internal degrees of freedom while the number of internal degrees of freedom of n-dodecane has been assumed to be in the range $N_{\text{int}} = 0$ to $N_{\text{int}} = 50$. The normalising factors do not affect the results of calculations of the final steady state of this system.

The results of calculations for the distribution of the number densities of n-dodecane ($n_d \equiv n_{C_{12}H_{26}}$) and nitrogen ($n_n \equiv n_{N_2}$), when the system has reached the steady state, are shown in Fig. 7. Three values of the number of internal degrees of freedom of n-dodecane ($N_{\text{int}} = 0,\ 3$ and 7) have been considered. As one can see from this figure, the distributions of both n-dodecane and nitrogen number densities visibly change when N_{int} increases from 0 to 3. These changes, however, become much smaller when N_{int} increases further from 3 to 7.

The results of calculations for the distribution of the normalised temperatures of n-dodecane and nitrogen, when the system reached the steady state, are shown in Fig. 8. As in the case of Fig. 7, three values of the number of internal degrees of freedom of n-dodecane (0, 3 and 7) have been considered. As one can see from this figure, the distributions of both n-dodecane and nitrogen noticeably change when N_{int} increases from 0 to 3. As in the case of Fig. 7, these changes become much less significant when N_{int} increases further from 3 to 7. The conclusions inferred from Figs. 7 and 8 are consistent with those inferred from Fig. 5 for a very different physical problem.

The difference between the values of gas temperature near the walls and the wall temperatures can be clearly seen in Fig. 8. This is a well known temperature jump in rarefied gases (e.g. [24]).

The plots of the normalised heat flux q between the plates versus N_{int} are shown in Fig. 9. We have used the normalisation factor

$$\rho_{C_{12}H_{26}} \left(R_{C_{12}H_{26}} T_0\right)^{3/2},$$

where $\rho_{C_{12}H_{26}}$ and $R_{C_{12}H_{26}}$ are the density and gas constant of n-dodecane respectively, T_0 is the initial dimensional temperature.

The cases of the above mentioned mixture of n-dodecane and nitrogen and pure n-dodecane have been considered. As follows from this figure, the changes in q at $N_{\text{int}} \geqslant 15$ are much smaller compared with the changes at $N_{\text{int}} < 15$. At $N_{\text{int}} > 25$, the values of q remain practically constant and do not depend on N_{int}.

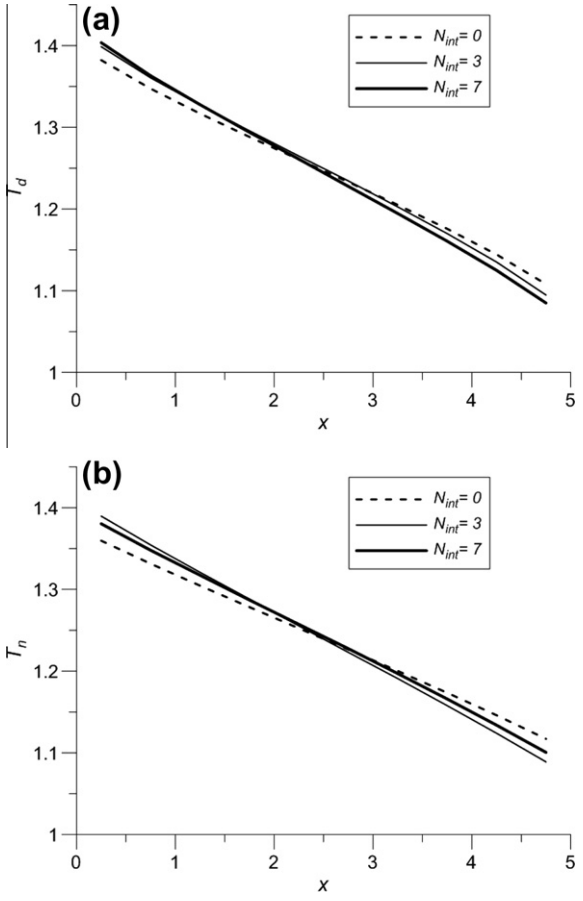

Fig. 8. The same as Fig. 7, but for the normalised temperatures of n-dodecane and nitrogen (T_d (a) and T_n (b)).

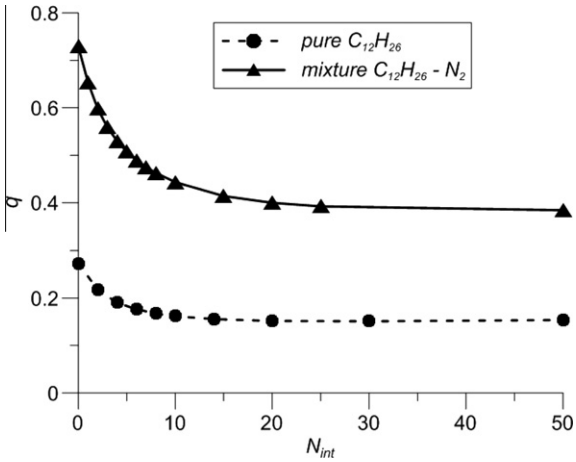

Fig. 9. Plots of the normalised heat flux q versus N_{int} for pure n-dodecane and the mixture of n-dodecane and nitrogen for the setup shown in Fig. 6.

3.3. Evaporation of n-dodecane into nitrogen

Let us consider two parallel plates, similar to those studied in the previous section, but at normalised temperatures $T_{w1} = T_{w2} = 1$; initially the space between these plates is filled with nitrogen at the normalised temperature $T = 1$ and number density $n_n \equiv n_{\text{N}_2} = 1$. The total amount of nitrogen in the system is assumed to be constant. As in the previous problem, the distance between the plates is taken equal to $L = 5\ell$. n-Dodecane is evaporated from the first plate in such a way that its normalised number density at the surface of this plate remains constant and equal to 1.5. Once n-dodecane reaches the right plate it fully condenses so that its number density at the surface of this plate remains equal to 0. This setup is schematically shown in Fig. 10.

As in the case of the previous problem, the calculations have been performed assuming that nitrogen has no internal degrees of freedom while the number of internal degrees of freedom of n-dodecane are assumed to be in the range $N_{\text{int}} = 0$ to $N_{\text{int}} = 50$.

The results of calculations for the distribution of the number densities of n-dodecane and nitrogen, when the system reached the steady state, are shown in Fig. 11. Four values of the number of internal degrees of freedom of n-dodecane ($N_{\text{int}} = 0,\ 3,\ 7$ and 10) have been considered. As one can see from this figure, the distributions of both n-dodecane and nitrogen number densities visibly change when N_{int} increases from 0 to 3. These changes, however, become smaller when N_{int} increases further from 3 to 7, and can be practically ignored when N_{int} increases from 7 to 10.

The plots of normalised mass flux j between the plates versus N_{int} are shown in Fig. 12. We have used the normalisation factor

$$\rho_{\text{C}_{12}\text{H}_{26}} \sqrt{R_{\text{C}_{12}\text{H}_{26}} T_0},$$

where the notations are the same as in the previous subsection.

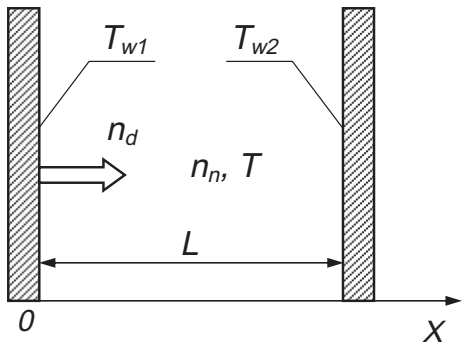

Fig. 10. A schematic presentation of the setup used for the analysis of the evaporation of n-dodecane into nitrogen. n-Dodecane is evaporated from the left-hand side plate kept at a temperature equal to T_{w1} and is fully condensed at the right-hand side plate kept at a temperature equal to T_{w2}. L is the distance between the plates; n_d and n_n are number densities of n-dodecane and nitrogen respectively; $T \equiv T(x)$ is the temperature between the plates.

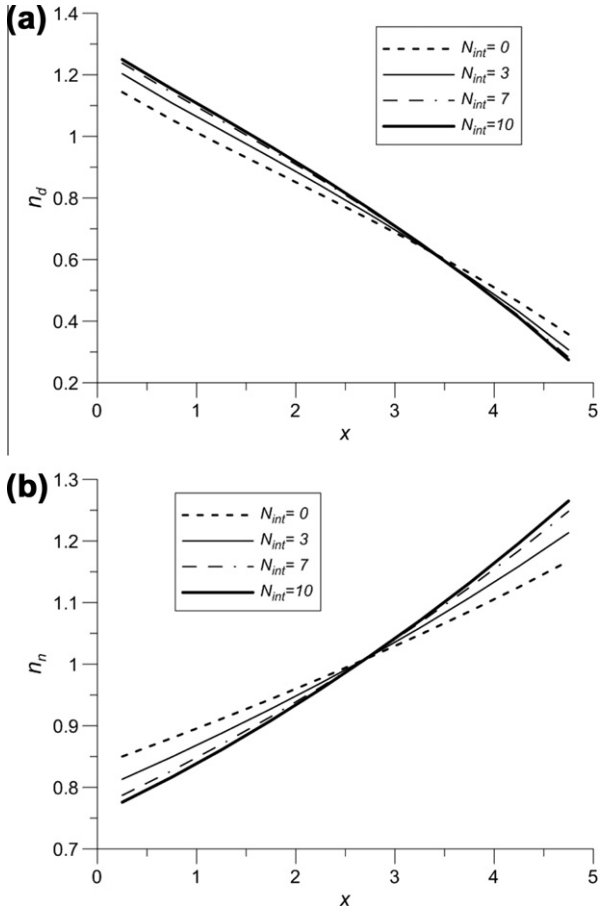

Fig. 11. Plots of n_d (a) and n_n (b) versus the distance x normalised by the mean free path ℓ for four values of N_{int} for the setup shown in Fig. 10. $x = 0$ shows the location of the left-hand side plate.

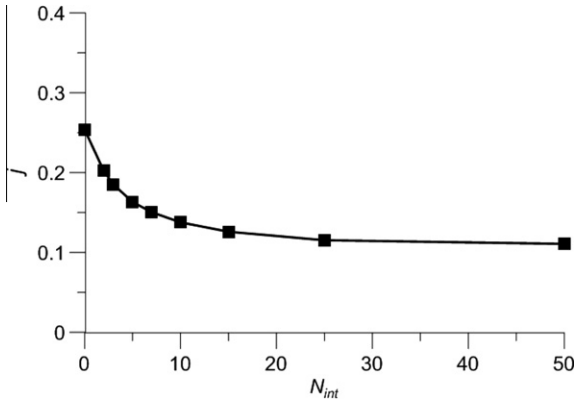

Fig. 12. Plots of the normalised mass flux of n-dodecane j versus N_{int} for the setup shown in Fig. 10.

As follows from this figure, the changes in j at $N_{\text{int}} \geqslant 15$ are much smaller compared with the changes at $N_{\text{int}} < 15$, as in the case of the previous problem. At $N_{\text{int}} > 25$, the values of j remain practically constant and do not depend on N_{int}.

The results presented in this section open the way for applying the method described in this paper to systems with arbitrarily large numbers of internal degrees of freedom by considering systems with relatively small numbers of these degrees of freedom. The number of internal degrees of freedom to be chosen would depend on the required accuracy of the solution.

4. Conclusions

A new approach to the solution of the Boltzmann equation, taking into account the effect of inelastic collisions, is suggested. This approach is based on the presentation of the collisions as the random (with uniform probability distribution) movement along a surface of an N-dimensional sphere, the squared radius of which is equal to the total energy of colliding molecules in the centre of mass reference system. The projection of a point on the surface of this sphere in each of N directions gives the root square of the kinetic energy in one of three directions in the physical space, or internal energy referring to one degree of freedom, of one of the colliding molecules. The kinetic energies of both colliding molecules in three directions are described by the first six dimensions of the system, and the remaining $(N-6)$ dimensions describe the internal energies. In contrast to the case of elastic collisions, the radius of the three-dimensional sphere in the momentum or velocity space describing the kinetic energies of both molecules changes after each collision. The probabilities of changes of all energies (kinetic and internal) after collision are assumed to be equal. If during the collision the net internal energy of molecules increases (decreases), this has to be compensated for by the decrease (increase) of the kinetic energies of molecules, and the radius of the corresponding sphere in the three-dimensional kinetic space decreases (increases). Following [29], we assume that the momenta of molecules after the collisions belong to an *a priori* chosen set of momenta, which are nodes in the momenta space. The changes of radii of the spheres in the kinetic space after collisions are calculated based on Korobov's sequences, enhanced by the randomisation of individual points.

The above mentioned new approach has been applied to three test problems: shock wave structure in nitrogen, one-dimensional heat transfer through a mixture of n-dodecane and nitrogen and one-dimensional evaporation of n-dodecane into nitrogen. In the first problem, the predictions of the model, taking into account the contribution of the rotational degrees of freedom, are shown to be close to experimental data and the predictions of the earlier developed model, based on a different approach to taking into account the effects of inelastic collisions. This problem has been generalised to a hypothetical case when the number of internal degrees of freedom of nitrogen (N_{int}) has been assumed to be in the range 0–10. It has been shown that the results visibly change when N_{int} is increased from 0 to 2, but remain practically unchanged for $N_{\text{int}} \geqslant 6$.

The predicted heat flux for the second problem has been shown not to depend on the number of internal degrees of freedom of the mixture N_{int} when this number exceeds about 15. In the third problem, the predicted mass flux of n-dodecane also remained almost unchanged for $N_{\text{int}} \geqslant 15$. These results open the way for considering systems with arbitrarily large numbers of internal degrees of freedom by reducing the analysis of these systems to the analysis of systems with relatively small numbers of internal degrees of freedom.

Acknowledgements

The authors are grateful to the EPSRC (Grant EP/H001603/1) (UK) and Russian Foundation for Basic Research (Grant 10-08-00614) for the financial support of this project.

References

[1] H. Alsmeyer, Density profiles in argon and nitrogen shock waves measured by the absorption of an electron beam, J. Fluid Mech. 74 (3) (1976) 497–513.
[2] V.V. Aristov, F.G. Tcheremissine, Direct Numerical Solution of the Boltzmann Equation, Computer Centre of the Russian Academy of Sciences, Moscow, 1992.
[3] J. Banasiak, M. Groppi, Solvability of linear kinetic equations with multi-energetic inelastic scattering, Reports Math. Phys. 52 (2) (2003) 235–253.
[4] D. Benedetto, E. Caglioti, The collapse phenomenon in one-dimensional inelastic point particle systems, Physica D 132 (1999) 457–475.
[5] T. Biben, Ph.A. Martin, J. Piasecki, Stationary state of thermostated inelastic hard spheres, Physica A 310 (2002) 308–324.
[6] C. Borgnakke, P.S. Larsen, Statistical collision model for Monte Carlo simulation of polyatomic gas mixture, J. Comput. Phys. 18 (4) (1975) 405–420.
[7] B.-Y. Cao, J.-F. Xie, S.S. Sazhin, Molecular dynamics study on evaporation and condensation of n-dodecane at liquid–vapour phase equilibria, J. Chem. Phys. 134 (2011) 164309.
[8] C. Croizet, A BGK model for a suspension of inelastic spheres, Math. Comput. Model. 41 (2005) 1379–1388.
[9] L. Ferrari, A. Carbognani, Differential kinetic equations for a Rayleigh gas with inelastic collisions, Physica A 251 (1998) 452–468.
[10] N. Fournier, S. Mischler, A spatially homogeneous Boltzmann equation for elastic, inelastic and coalescing collisions, J. Math. Pures Appl. 84 (2005) 1173–1234.
[11] G. Furioli, A. Pulvirenti, E. Terraneo, G. Toscani, Convergence to self-similarity for the Boltzmann equation for strongly inelastic Maxwell molecules, Ann. I. H. Poincaré AN 27 (2010) 719–737.
[12] V. Kharchenko, N. Balakrishnan, A. Dalgarno, Thermalization of fast nitrogen atoms in elastic and inelastic collisions with molecules of atmospheric gases, J. Atmos. Sol.-Terres. Phys. 60 (1) (1998) 95–106.
[13] N.M. Korobov, Trigonometric Sums and Their Applications, Nauka Publishing House, Moscow, 1989 (in Russian).
[14] K. Koura, Improved null-collision technique in the direct simulation Monte Carlo method: application to vibrational relaxation of nitrogen, Comput. Math. Appl. 35 (1/2) (1998) 139–154.
[15] G.M. Kremer, A.W. Silva, G.M. Alves, On inelastic reactive collisions in kinetic theory of chemically reacting gas mixtures, Physica A 389 (2010) 2708–2718.
[16] A.P. Kryukov, V.Yu. Levashov, S.S. Sazhin, Evaporation of diesel fuel droplets: kinetic versus hydrodynamic models, Int. J. Heat Mass Transfer 47 (12–13) (2004) 2541–2549.
[17] R. Lambiotte, M. Ausloos, L. Brenig, J.M. Salazar, Energy and number of collision fluctuations in inelastic gases, Physica A 375 (2007) 227–232.
[18] S.P. Popov, F.G. Tcheremissine, Conservative method of the solution of the Boltzmann equation for centrally symmetrical interaction potentials, Comput. Math. Math. Phys. 39 (1999) 163–176.
[19] A. Raines, Study of a shock wave structure in gas mixtures on the basis of the Boltzmann equation, Eur. J. Mech. 21 (2002) 599–610.
[20] A. Santos, Transport coefficients of d-dimensional inelastic Maxwell models, Physica A 321 (2003) 442–466.

[21] A. Santos, A simple model kinetic equation for inelastic Maxwell particles, in: M.S. Ivanov, A.K. Rebrov (Eds.), Proceedings of the 25th International Symposium on Rarefied Gas Dynamics, July 21–28th 2006, St Petersburg, Russia, Publishing House of the Siberian Branch of the Russian Academy of Sciences, Novosibirsk, 2006, pp. 191–196. ISBN 978-576-9209-246.
[22] S.S. Sazhin, Advanced models of fuel droplet heating and evaporation, Prog. Energy Combust. Sci. 32 (2) (2006) 162–214.
[23] S.S. Sazhin, I.N. Shishkova, A kinetic algorithm for modelling the droplet evaporation process in the presence of heat flux and background gas, Atom. Sprays 19 (5) (2009) 473–489.
[24] S.S. Sazhin, V.V. Serikov, Rarefied gas flows: hydrodynamic versus Monte Carlo modelling, Planet. Space Sci. 45 (3) (1997) 361–368.
[25] S.S. Sazhin, P. Wild, C. Leys, D. Toebaert, E.M. Sazhina, The three temperature model for the fast-axial-flow CO_2 laser, J. Phys. D: Appl. Phys. 26 (1993) 1872–1883.
[26] S.S. Sazhin, P. Wild, E.M. Sazhina, M. Makhlouf, C. Leys, D. Toebaert, The three dimensional modelling of the processes in the fast-axial-flow CO_2 laser, J. Phys. D: Appl. Phys. 27 (3) (1994) 464–469.
[27] S.S. Sazhin, I.N. Shishkova, A.P. Kryukov, V.Yu. Levashov, M.R. Heikal, Evaporation of droplets into a background gas: kinetic modelling, Int. J. Heat Mass Transfer 50 (2007) 2675–2691.
[28] S.S. Sazhin, I.N. Shishkova, M.R. Heikal, Kinetic modelling of fuel droplet heating and evaporation: calculations and approximations, Int. J. Eng. Syst. Model. Simul. 2 (3) (2010) 169–176.
[29] I.N. Shishkova, S.S. Sazhin, A numerical algorithm for kinetic modelling of evaporation processes, J. Comput. Phys. 218 (2) (2006) 635–653.
[30] A. Sizhuk, S. Yezhov, The dynamic theory for the inelastically colliding particles, J. Mol. Liq. 127 (2006) 84–86.
[31] T. Stoecklin, A. Voronin, H–N_2 inelastic collision dynamics on new potential energy surface, Chem. Phys. 331 (2007) 385–395.
[32] F.G. Tcheremissine, Direct numerical solution of the Boltzmann equation, in: M.S. Ivanov, A.K. Rebrov (Eds.), Proceedings of the 25th International Symposium on Rarefied Gas Dynamics, July 21–28th 2006, St Petersburg, Russia, Publishing House of the Siberian Branch of the Russian Academy of Sciences, Novosibirsk, 2006, pp. 677–685. ISBN 978-576-9209-246.
[33] I.S. Tilinin, Impact-parameter dependence of inelastic energy losses in slow atom–atom collisions, Nucl. Instrum. Methods Phys. Res. B 115 (1996) 102–105.
[34] J.-F. Xie, S.S. Sazhin, B.-Y. Cao, Molecular dynamics study of the processes in the vicinity of the n-dodecane vapour/liquid interface, Phys. Fluids 23 (2011) 112104, http://dx.doi.org/10.1063/1.3662004.
[35] V.A. Zenevich, G.D. Billing, G. Jolicard, Vibrational–rotational energy transfer in H_2–H_2 collisions II. The relative roles of the initial rotational excitation of both diatoms, Chem. Phys. Lett. 312 (1999) 530–535.